Domain Sizes Determination for Styrene−Isobutylene Block Copolymer Systems Using Solid-State NMR Spectroscopy

Claudiu Neagu,[†] Judit E. Puskas,[‡] Marsha A. Singh,[§] and Almeria Natansohn*[,†]

Department of Chemistry, Queen's University, Kingston, Ontario, Canada K7L 3N6; Department of Chemical and Bio-Chemical Engineering, University of Western Ontario, London, Ontario, Canada N6A 5B8; and Department of Physics, Queen's University, Kingston, Ontario, Canada K7L 3N6

Received November 23, 1999

ABSTRACT: Solid-state NMR techniques were used to evaluate the sizes of the dispersed domains and the interface between the minor and the major phase in heterogeneous block copolymer systems with a relatively poor degree of ordering. Proton spin−lattice relaxation measurements and spin diffusion experiments were carried out on five samples of linear and star block copolymers of styrene, styrene-*co*-indene, and isobutylene. The morphology of the dispersed phase was considered cylindrical for all samples. The diameters of the dispersed cylinders were found to range between 7.9 and 48.5 nm for the linear samples and 22.6 nm for the star block copolymer sample. The thickness of the interface was estimated to be between 1.0 and 1.3 nm for all samples. SAXS measurements were employed to confirm the validity of the NMR data analysis.

1. Introduction

Thermoplastic elastomers are becoming increasingly attractive as manufacturing materials due to the possibility of tailoring them for a specific set of desired properties. The use of thermoplastic elastomers in new applications requires the ability to customize polymer materials with particular physical properties such as tensile strength, torsional moduli, extensibility, density, and long-term stability[1] to name just a few of them. The mechanical properties of the thermoplastic elastomers are related to the sizes of the dispersed domains and to the thickness of the interface between the minor and the major component. Therefore, to engineer these materials for a particular set of end use properties, a thorough understanding of the structure−property relationship is essential. This can be achieved through a set of methods currently employed to investigate the scale of heterogeneity for these materials. Differential scanning calorimetry (DSC) can be used in the case of systems consisting of polymers with glass transition temperatures differing by at least 25 K.[2] This method gives qualitative information about miscibility for domain sizes down to about 10 nm. Small-angle X-ray scattering (SAXS) is used for systems with a good electron density contrast between components. Transmission electron microscopy (TEM) can be used to reveal the morphology of the system, but its reliability in determining the domain sizes is restricted to systems with a good degree of ordering. TEM does not provide information about the thickness of the interface between the minor and the major components. Scanning electron microscopy (SEM) does not allow accurate evaluation of domain sizes smaller than a few hundreds of nanometers and, like TEM, cannot provide information about the thickness of the interface. With fluorescence spectroscopy both the domain sizes and thickness of the interface can be determined. The shortcoming of this method is that it requires sample modification.

A suitable method to characterize the microstructure of heterogeneous polymer systems is solid-state NMR.[3] NMR spectroscopy applied to solid materials leads to valuable information regarding composition, molecular mobility, and molecular order[4] and, therefore, is capable of probing chemical or physical heterogeneities down to a scale below 1 nm.[5] Additionally, this method has the advantage of retrieving information about phase separation in a noninvasive manner and without any sample modification. Hence, it could also use samples taken directly from the industrial stream to be analyzed without any further modification. Solid-state NMR can determine simultaneously domain sizes and interface thickness. Recent two-dimensional NMR techniques have been used to determine phase sizes and interface thickness of heterogeneous polymer samples on a range from about 1 nm to above 200 nm,[4] the upper limit depending on the chemical nature of the polymers that form the blocks.

The materials of interest in this study are thermoplastic elastomers: block copolymers containing a midsegment of rubber (polyisobutylene, PIB) flanked by glassy outer segments of polystyrene (PS) or poly(styrene-*co*-indene) (PSI). On the basis of the different solubility parameters of the polymer blocks, listed in Table 1, these materials are expected to associate into micellar aggregates.

The dispersed phases may be, for example, spherical, rodlike, or disks (lamellae), depending on the molecular features and volume fraction of the minor component.[6] For this kind of material, the morphology, the phase sizes of the reinforcing polymer, and the near-neighbor distance can be controlled by synthesis.

2. Experimental Section

2.1. NMR Spectroscopy. 2.1.1. ^{13}C NMR Spectroscopy. All experiments were performed on a Bruker ASX 200 NMR spectrometer with field strength of 4.7 T or a 200 MHz resonant frequency of protons. The spectrometer was equipped with a standard Bruker ^{1}H−^{13}C double-resonance MAS probe head. The diameter of the spinner was 7 mm. The cross polarized magic angle spinning (CP-MAS) ^{13}C spectra were

[†] Department of Chemistry, Queen's University.
[‡] University of Western Ontario.
[§] Department of Physics, Queen's University.

10.1021/ma991974i CCC: $19.00
Published on Web 07/13/2000

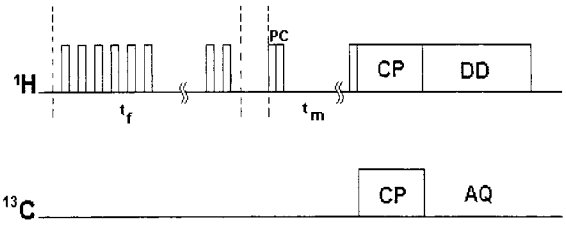

Figure 1. Pulse sequence for dipolar filter experiments.[8]

Table 1. Some Physical Properties of the Blocks

block	PS	PSI	PIB
density [g/cm^3]	1.06	1.06	0.92
solubility parameter [(cal/cm^3)^2]	9.13	9.22	7.85
spin diffusion coeff [nm^2/ms]	0.80	0.80	0.15

acquired at spinning speeds of the sample rotor between 2.7 and 3.3 kHz and with high power proton decoupling during acquisition. The 90° pulse width was 4.2 μs. A variable contact-time experiment was run for all samples. The maximum cross-polarization efficiency was at 1.5 ms contact time for the rigid component and at about 0.5 ms for the rubber. A contact time of 0.75 ms was used in the regular CP-MAS experiments.

Inversion recovery experiments were carried out to estimate the spin−lattice relaxation times in the laboratory frame. A sequence consisting of a 90° pulse on the proton channel followed by a variable spin locking pulse was used to evaluate the spin−lattice relaxation times in the rotating frame.[7] The frequency of the spin lock field was 59.5 kHz.

For spin diffusion experiments polarization gradients were generated by exploiting proton line width differences. The delay between the 90° pulses applied in the dipolar filter sequence[8] was of 12 μs, and the pulse train was repeated six times in each of the spin diffusion experiments. Also, immediately after the dipolar filter, pulses of 0° and 180° were applied alternatively, i.e., phase cycling, to minimize the effects of proton spin−lattice relaxation. Each spectrum was acquired with 1000−2000 transients and a recycling delay of 2.5 s. The dipolar filter pulse sequence is shown in Figure 1.

2.1.2. ^{1}H NMR Spectroscopy. A CRAMPS probe (Doty Scientific) designed to house 5 mm spinners was used. Spectrometer tuning on cylindrical samples of water, adamantane, and malonic acid was performed according to published procedures.[9] For each of the proton spectra 16−32 transients were collected. Spin−spin relaxation measurements were done using the Carr−Purcell−Meiboom−Gill (CPMG)[10,11] spin-echo pulse sequence. The delay between acquiring two consecutive points of the decaying signal was 5 μs. The acquired signal was averaged over 8−64 transients.

2.2. SAXS Measurements. SAXS data were obtained at the synchrotron facility of the Laboratório Nacional de Luz Sínchrotron (LNLS) in Campinas, Brazil. The SAXS beamline D11A was used. A 1-dimensional gas-phase detector was used with a sample-to-detector distance of 1.5 m and a wavelength of 1.6 Å. Five minute exposures were used with a background correction provided by measuring the scattering in the absence of the sample. The background data were normalized using transmission ratios with a NaI scintillation detector placed in line with the main beam after Co and Al attenuators. The possibility of detector artifacts occurring at positions near the primary beam was noted. However, the SAXS data interpretation presented later exclude the lowest scattering angles.

2.3. Thermal Analysis. Thermal analysis for both homopolymer and copolymer samples was performed on a Mettler TC 10A differential scanning calorimeter at a heating rate of 10 °C/min.

2.4. Materials. Each block copolymer sample was characterized from the point of view of structure and composition using both size exclusion chromatography (SEC) and NMR data. The molecular weights of the block copolymers were estimated SEC with respect to polystyrene standards. The composition of the copolymers was determined by solution ^{1}H NMR. The molecular weights of the blocks were calculated from composition data. These polymer samples were synthesized via cationic polymerization. Composition and number-average molecular weights of the end blocks and of the entire copolymer are presented in Table 2. The chemical structure and molecular architecture of the samples are sketched in Figure 2. Additionally, homopolymer samples of PIB, PS, and polyisoprene (PI) were used as reference. The average molecular weights and the polydispersity indices for the PS, PIB, and PI samples are also summarized in Table 2. The PS sample was purchased from Aldrich Chemicals Co. For purposes of SAXS measurements sample L26 was heated to about 80 °C for about 20 min.

Table 2. Composition of the Samples and Number-Average Molecular Weights

sample	wt fraction of rigid component	av M_n of rigid block [$\times 10^3$ g/mol]	av M_n of entire sample [$\times 10^3$ g/mol]	polydispersity indices
L211	0.13	8.6	130	1.3
L216	0.19	18.1	185	1.3
ST83	0.26	12.0	138	1.4
L26	0.13	6.5	98	1.5
L23	0.31	15.5	99	1.4
PI	N/A	N/A	84	1.02
PIB	N/A	N/A	1412	1.1
PIB	N/A	N/A	375	1.2
PS	N/A	N/A	29.3[a]	N/A

[a] Viscosity average.

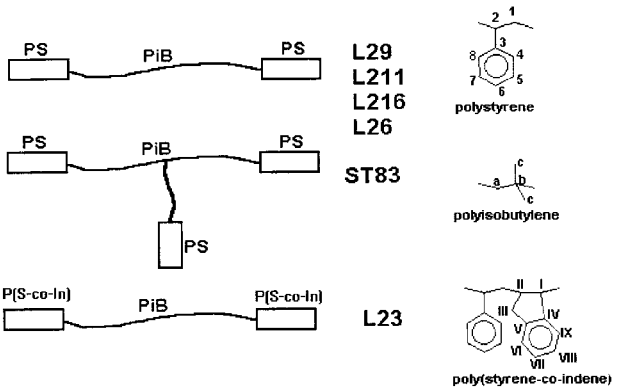

Figure 2. Molecular architecture of the block copolymers.

Some of the physical properties of the homopolymers that form the blocks, i.e., densities, spin diffusion coefficients, and solubility parameters, are presented in Table 1. Values for the densities of the blocks were taken from the literature,[12,13] except for PSI whose density was assumed to be the same as the density of PS. The interaction parameter between the polymer blocks was quantified in relation with their solubility parameters. Because neither PS (PSI) nor PIB is known to exhibit strong intermolecular interactions, their solubility parameters were calculated from group molar attraction constants.[12]

The values of glass transition temperatures (T_g's) of the polymers that form the blocks (−70 °C for PIB, 109 °C for PS, and 158 °C for PSI) were determined experimentally using thermal analysis (DSC).

3. Results

^{13}C CP− MAS spectra of the samples L26 and L23 are presented in Figure 3. Peak assignments are shown using the identification of the carbons from Figure 2. Since no suppression of spinning sidebands was employed, signals assigned to the rigid component, i.e., component with a large chemical shift anisotropy, appear across the spectrum at multiples of the spinning frequency (SSB). The frequency of the rotor was chosen in such a way that spinning sidebands did not overlap with the isotropic peaks of interest.

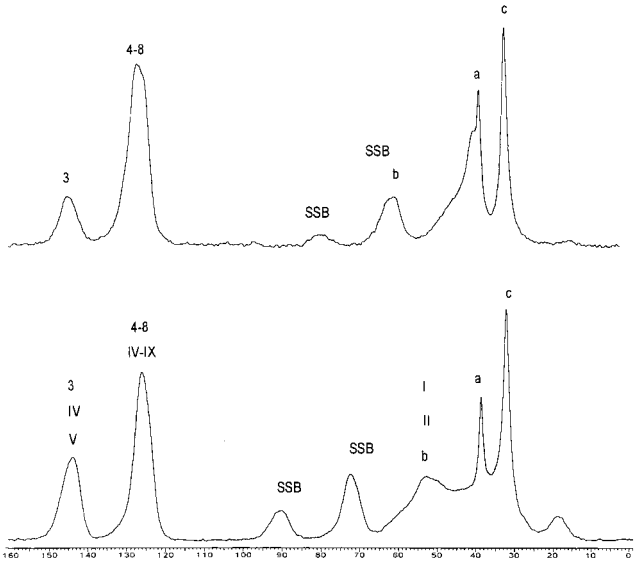

Figure 3. CP-MAS spectra of (a) sample L26 and (b) sample L23.

Table 3. (^{1}H) Spin−Lattice Relaxation Time Constants [ms]

sample	T_1 rigid comp	T_1 matrix	$T_{1\rho}$ rigid comp	$T_{1\rho}$ matrix
PS	1600		7.6	
PIB		150		0.30
L211	295	182	6.0	0.97
L216	340	178	6.7	1.01
ST83	330	160	6.10	0.40
L26	290	170	5.7	0.50
L23	340	175	18.50	0.70

3.1. Measurements of Proton Spin−Lattice Times. Measurements of proton spin−lattice times in both laboratory frame (T_1) and rotating frame ($T_{1\rho}$) were done for the block copolymer samples as well as for PIB and PS homopolymers. These results are presented in Table 3.

As seen in Table 3, both (^{1}H) spin−lattice relaxation times in the rotating and the laboratory frame measured in the block copolymer systems differ from those of the homopolymers. For all the samples it appears that spin−lattice relaxation times are influenced by spin diffusion. The distinct (^{1}H) T_1 and (^{1}H) $T_{1\rho}$ values of the block components of the same sample show that the systems are phase-separated.[14] It seems appropriate to assume that the polymer systems under investigation are heterogeneous at a scale above 1 nm.[4] Because spin diffusion changes the values of the proton T_1's of the blocks to values between the proton T_1's of PS and PIB, the domains are considered to be smaller than a few hundreds of nanometers. Therefore, the sizes of the dispersed domains are expected to be between a few nanometers and a few tens of nanometers.

3.2. Spin Diffusion Measurements. Domain sizes and interface thickness could be determined using the features of the spatial transfer of magnetization along the *z*-axis between dipolar-coupled spins during mixing and, where applicable, during CP times.

3.2.1. Determination of Spin Diffusion Coefficients. The transfer of magnetization within the homogeneous domains was quantified in relation to the spin diffusion coefficients (*D*'s), i.e., the rates of magnetization transfer through each of the polymer phases. The spinning frequencies in all spin diffusion experiments were always of a few kilohertz, i.e., from 1.5 to about 3.5 kHz.

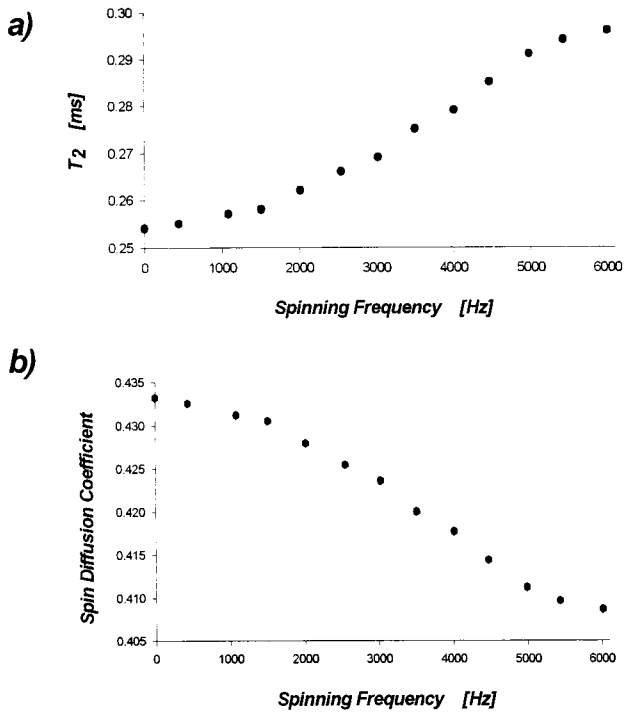

Figure 4. (a) Measured spin−spin relaxation times and (b) calculated spin diffusion coefficients in nm^2/ms of PIB vs rotor frequency.

Evaluations of the spin diffusion coefficients shown in eq 1 as suggested by Clauss et al.[3] were not attempted due, for the particular case of PIB, to the impossibility of resolving the proton peaks even using the strongest homonuclear decoupling the hardware allowed. It was concluded that the use of eq 1 would, therefore, lead to overestimating the spin diffusion coefficients.

$$D \approx \Delta\nu_{1/2}(r_{HH})^2 \qquad (1)$$

In eq 1 r_{HH} represents the average inter-proton distance. The dependence of the spin diffusion coefficients of the transverse relaxation rate T_2^{-1} was exploited as suggested by Mellinger et al.[11,15] Equation 2 shows the dependence of the spin diffusion coefficient in nm^2/ms for the range $0 < 1/T_2 < 1000$ Hz.

$$D(T_2) = 8.167 \times 10^{-6} T_2^{-1.5} + 0.007 \qquad (2)$$

The variations of the measured proton spin−spin relaxation times and of the calculated spin diffusion coefficients of PIB with the spinning frequency are shown in Figure 4. The value of the spin diffusion coefficient of PIB used in further calculations was chosen according to the spinning speed of the sample rotor at which the experiment was carried out (Figure 4b).

The value of the spin diffusion coefficient for PS was also determined using experimental data from proton spin−spin relaxation experiments. The value calculated according to the equation proposed by Mellinger et al. for the case of T_2^{-1} between 1000 and 3600 Hz, i.e., eq 3, is of 0.67 nm^2/ms.

$$D(T_2) = 4.4 \times 10^{-5} T_2^{-1} + 0.24 \qquad (3)$$

The T_2^{-1} value measured for PS exceeded 3.6 kHz, and

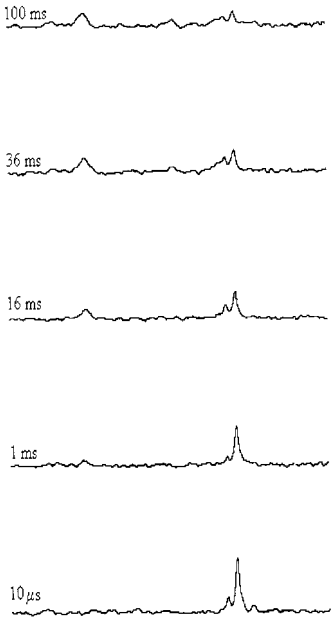

Figure 5. Spin diffusion spectra for sample L26.

therefore, the value calculated with the semiempirical equation suggested by Mellinger et al. was subjected to further verification. This was done using spin diffusion experiments run on a PS homopolymer sample, employing the chemical shift filter for building up a magnetization gradient between the aromatic and the aliphatic protons. A value of 0.8 nm^2/ms was determined for the spin diffusion coefficient of PS. This value was found to agree with previously published data.[16] This latter value was used in the calculations.

3.2.2. Simulation of the Magnetization Transfer. Spin diffusion experiments employing the dipolar filter pulse sequence[3] were run at room temperature for each block copolymer sample. The working temperature is at least 70 K below the highest T_g as recommended by Landfester and Spiess for a good performance of the dipolar filter.[17] For all spin diffusion experiments involving the dipolar filter for selection, the recovery of the magnetization belonging to the rigid component was always monitored for the ^{13}C aromatic signal at a chemical shift of about 127 ppm. The dipolar filter was repeated until the magnetization of the dispersed polymer was suppressed. A stack of plots for spin diffusion experiments is shown in Figure 5. These particular spectra were acquired on sample L26.

The time axis of the experimental data was scaled up by adding half of the contact (CP) time, considering that the magnetization transfer occurs with half the coupling strength during the cross-polarization period. Initial results for domain sizes were obtained using the method of initial-rate approximation done according to eq 4.[3]

$$d_A = \frac{\rho_{HA}\phi_A + \rho_{HB}\phi_B}{\phi_A\phi_B}\,\frac{4\epsilon\phi_A}{\sqrt{\pi}}\,\frac{\sqrt{D_A D_B}}{\rho_{HA}D_A + \rho_{HB}D_B}\,\sqrt{t^*_m} \quad (4)$$

The domain size (d) of the dispersed phase (A) could be a diameter or a thickness depending on the dimensionality of the system (ϵ). System dimensionality is defined as the number of molecular dimensions in tridimensional space coordinates; i.e., it would have values of 1 for lamellar, 2 for cylindrical, and 3 for spherical morphologies. The values of the volume fractions (ϕ) and those of the proton densities (ρ_H) were based on the number of protons and the molecular weight of the structural units and the densities of the PIB, PS, and PSI homopolymers. The value for mixing time, t^*_m, used in eq 3 is given by the intersection of the slope of the initial growth of the recovering magnetization with the slope of the tail of the same curve. For sample L26, a graphical evaluation of the mixing time used in eq 2 is shown in Figure 6.

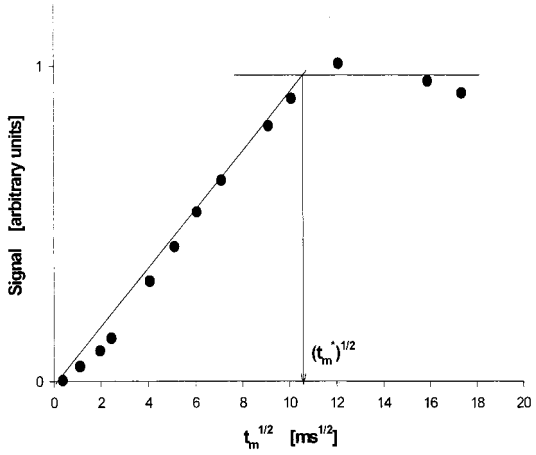

Figure 6. Initial rate approximation for sample L26.

Toward the end of the spin diffusion process, the spin−lattice relaxation becomes dominant, and the use of phase cycling is primarily affecting the tail of the spin diffusion curve. To obtain a plateau for the tail of the spin diffusion curve, the values of the experimental data were corrected with a spin−lattice relaxation term that accounts for the effects of phase cycling. The correction term is $\exp(t_m/T_1)$,[18] where t_m is the mixing time and T_1 is the intrinsic value of the spin−lattice relaxation time, i.e., the value of the proton T_1 of PS or PSI. The characteristic size (L) of the matrix (B), the distance between the centers of two closest neighboring dispersed domains, i.e., long period, is calculated initially with eq 5.[19]

$$L = d_A/\sqrt{1 - \phi_B} \quad (5)$$

The values of domain sizes and long periods are presented in Table 4 for the block copolymer samples.

The transfer of magnetization was also simulated to include the effects of the spin−lattice relaxation in the mathematical model by numerical integration of eq 6.[20] For this approach, the experimental data did not require adjusting as in the initial-rate approximation method presented above because the mathematical model, in this instance, also considers the phase cycling.

$$\frac{\partial c(r,t)}{\partial t} = D\Delta^2 c(r,t) + \frac{c^\infty - c(r,t)}{T_1} \quad (6)$$

The quantity $c(r,t)$ represents the instantaneous magnetization, while c^∞ is the equilibrium value of the monitored magnetization.

3.3. Results from NMR Measurements. For all the heterogeneous polymer systems under investigation, the morphology of the dispersed domains was considered cylindrical on the basis of volume fraction considerations and on TEM analysis published for similar samples.[21] The numerical simulation results do not differ significantly from those calculated with the initial rate approximation. The numerical integration of eq 6 is

Table 4. Domain Sizes and Interface Thickness

		initial rate approximation		numerical integration			data corrected; cf. eq 7	
sample	morphology	diameter [nm]	*L* [nm]	diameter [nm]	interface [nm]	*L* [nm]	diameter [nm]	*L* [nm]
L211	cylindrical	12	34	7.0	1.3	24.5	7.9	26.1
L216	cylindrical	15	35	22.0	1.1	55.0	24.8	59.9
ST83	cylindrical	17	34	20.0	1.2	44.0	22.6	47.7
L26	cylindrical	24	68	17.0	1.0	48.0	19.2	56.7
L23	cylindrical	43	81	43.0	1.0	80.0	48.5	90.9

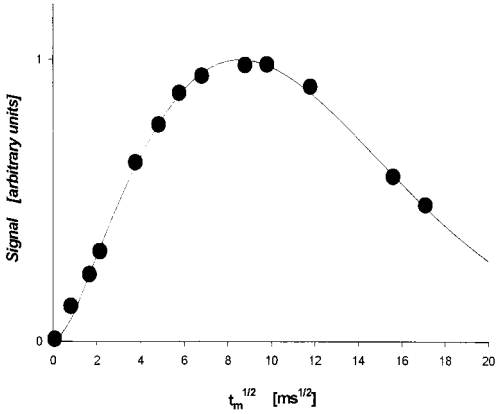

Figure 7. Spin diffusion experimental and simulated data for the recovery through spin diffusion of the PS line for sample L26.

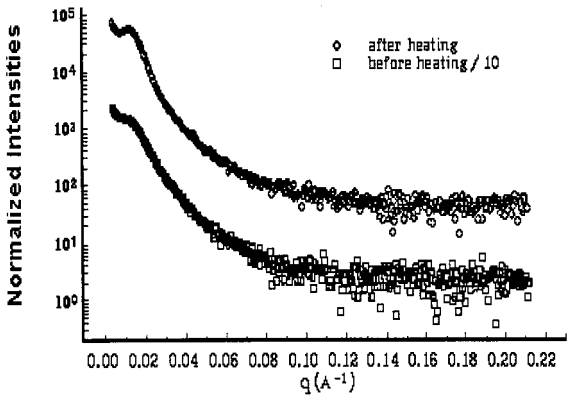

Figure 8. SAXS measurements on sample L26.

particularly very useful for obtaining information about the interface thickness. The interface was considered as a linear change in the composition between the two polymers.[22] (^{1}H) T_1 and D were assumed to change across the interface length in the same linear fashion. The presence of the interface in the heterogeneous polymer system is responsible for the sigmoidal trend of the spin diffusion curve.[23] Modifying the boundary conditions when solving eq 4 with numerical methods allows the evaluation of the interface thickness. Simulation of the spin diffusion curve for sample L26 shows the best fit of experimental results for a diameter of the dispersed cylinders of PS of 17 nm and a thickness of the interface of 1.0 nm (Figure 7). The domain sizes, interface thickness, and long periods were determined in similar fashion for all the samples. The values of domain sizes obtained by numerical integration of eq 6 were multiplied by a correction factor that transforms the simulated square profile (d_{NMR}) into a circular one (d'). For the assumed cylindrical morphology the calculation was done according to eq 7.[24]

$$d = 2d_{NMR}/\sqrt{\pi} \tag{7}$$

The interface thickness is considered unchanged by this correction. L is recalculated through numerical integration according to the thickness of the interface and the last calculated values of the diameters of the dispersed cylinders. The diameters of the dispersed cylinders corrected as shown in eq 7, and the long periods calculated accordingly are also presented in Table 4. The values of L, estimated with eq 5, are always smaller than those obtained by numerical integration of eq 6. This is expected since eq 5 does not take into account the volumes of the polymers that make the interface.

3.4. Results from SAXS Measurements. To check the accuracy of the NMR results presented earlier, SAXS analysis was attempted on sample L26 as an alternative method of investigation. The reason for choosing L26 was its relatively small volume fraction of the rigid component, which might make arguable the assumption made for this sample of exhibiting cylindrical morphology. SAXS measurements on this samples were difficult due to the poor degree of ordering in the heterogeneous material and because polymers are intrinsically poor scatterers. However, the possibility of detector artifacts occurring in the vicinity of the beamstop is not relevant to the interpretation of SAXS data presented. The interaction peak that is observed in Figure 8 responds to heating indicating enhanced phase separation upon annealing.

Semilog plots of the data show that the primary peak is located at about 0.0125 Å^{-1} as shown in Figure 8. The absence of higher-order peaks is taken as evidence of very limited ordering in the system. An average near-neighbor distance of 62.8 nm was calculated with an estimated uncertainty of about 7%.[25] The scattering angle is given in terms of $q = (4\pi/\lambda)\sin(\theta)$, where 2θ is the scattering angle and λ is the wavelength of the radiation used, i.e., 1.6 Å.

Porod analysis[26] was done on data corrected for detector inhomogeneity and parasitic scattering. The L26 sample does not show evidence of well-defined particles. The annealed L26 sample shows an enhanced degree of order. Preliminary Porod analysis on background corrected data of the annealed sample led to the conclusion that the interface is relatively sharp and not resolvable within the resolution of the measurement.

4. Discussion

The domain sizes of the dispersed phase appear to be proportional to the molecular weight of the minor component, raised to a power of about $^2/_3$. This relationship is reproduced by eq 8.[13]

$$d = kM^{\alpha} \tag{8}$$

k is a proportionality constant which depends on the nature of the dispersed polymer and on the morphology. The plot shown in Figure 9 depicts the dependence of the domain sizes on the molecular weight of the minor

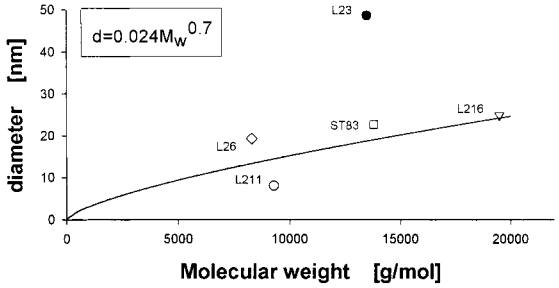

Figure 9. Domain size dependence on weight fraction of the dispersed phase.

component. The values for k and α can be read from the equation presented in the inset.

A value for α of 0.66 has been reported for a series of block copolymer systems comprised of units of styrene and isoprene.[27] The same value for α, i.e., 0.66, has been determined by Jack et al.[24] on block copolymers of styrene and isoprene. The value of 0.7 obtained for α for our samples appears to be consistent with data published on other thermoplastic elastomers.

The L23 sample appears to be an exception from this dependence. This is, possibly, due to the different chemical nature of the end polymer blocks. For this sample, there is a greater difference between the solubility parameters of its blocks.

Figure 9 shows deviations of the values of the diameters of the dispersed phase from the values predicted by eq 8, especially at lower molecular weights of the end blocks. This is probably due to the fairly large distributions of molecular weights of the polymer blocks and also because these distributions of molecular weights are different from one sample to another. In addition, the sizes of the dispersed domains do not appear to be influenced by the molecular architecture of the block copolymers.

5. Conclusions

Solid-state NMR proved successful in determining domain sizes and interface thickness in heterogeneous polymer systems with a poor degree of ordering. The interface thickness for all the heterogeneous samples was estimated to be between 1 and 1.3 nm. This range of values could be due to differences in polydispersity indices but could also reflect the inaccuracies of the method. The diameters of the dispersed cylinders were found between 7.9 and 48.5 nm for the linear samples. For the star-block copolymer the diameter of the dispersed cylinders was calculated to be 22.6 nm with an estimated uncertainty of less than 2 nm. The results by NMR and SAXS measurements appear to be consistent. For example, for sample L26, the distance between nearest-neighboring domains calculated from NMR data is 56.7 nm and is 62.8 nm calculated from SAXS data. Given the inherent experimental errors associated with both characterization methods, these results are considered to be in agreement. Therefore, the validity of the NMR method and the assumption for cylindrical morphologies for the block copolymer samples were confirmed.

The domain sizes of the dispersed phase display proportionality to the molecular weight raised at a power of about $^2/_3$. This dependence agrees with both experimental and theoretically predicted data for similar thermoplastic elastomers.[24,27]

Acknowledgment. NSERC and ESTAC are acknowledged for partial funding of this project. C.N. thanks Dr. Jiahu Wang and Dr. K. S. Jack for valuable discussions regarding the NMR experiments.

References and Notes

(1) *Multiphase Polymers: Blends and Ionomers*; ACS Symposium Series; Utracki, L. A., Weiss, R. A., Eds.; Maple Press: York, PA, 1988.
(2) Kaplan, D. S. *J. Appl. Sci.* **1976**, *20*, 2615.
(3) Clauss, J.; Schmidt-Rohr, K.; Spiess, H. W. *Acta Polym.* **1993**, *44*, 1.
(4) Schmidt-Rohr, K.; Spiess, H. W. In *Multidimensional Solid-State NMR and Polymers*; Academic Press: London, 1994.
(5) Cai, W. Z.; Schmidt-Rohr, K.; Egger, N.; Gerhartz, B.; Spiess, H. W. *Polymer* **1993**, *34*, 267.
(6) Matsen, M. W. *Macromolecules* **1995**, *28*, 5765.
(7) Voelkel, R. *Angew. Chem., Int. Ed. Engl.* **1988**, *27*, 1468.
(8) Clauss, J.; Schmidt-Rohr, K.; Adam, A.; Boeffel, C.; Spiess, H. W. *Macromolecules* **1992**, *25*, 5208.
(9) Jackson, P.; Harris, R. K. *Magn. Reson. Chem.* **1988**, *26*, 1003.
(10) Meiboom, S.; Gill, D. *Rev. Sci. Instrum.* **1958**, *29*, 688.
(11) Mellinger, F.; Wilhelm, M.; Spiess, H. W. *Macromolecules* **1999**, *32*, 4686.
(12) *Polymer Handbook*, 2nd ed.; Brandrup, J., Immergut, E. H., Eds.; John Willey and Sons: New York, 1975.
(13) Sperling, L. H. In *Polymeric Multicomponent Materials*; John Willey & Sons: New York, 1997.
(14) Havens, J. R.; VanderHart, D. L. *Macromolecules* **1985**, *18*, 1663.
(15) Mellinger, F.; Wilhelm, M.; Spiess, H. W.; Baumstark, R.; Haunschild, A. *Macromol. Chem. Phys.* **1999**, *200*, 719.
(16) Landfester, K.; Boeffel, C.; Lambla, M.; Spiess, H. W. *Macromolecules* **1996**, *29*, 5972.
(17) Landfester, K.; Spiess, H. W. *Macromol. Rapid Commun.* **1996**, *17*, 875.
(18) Friebel, S.; Harris, R. K.; Kenwright, A. M. *Magn. Reson.* **1997**, *35*, 290.
(19) Schmidt-Rohr, K.; Clauss, J.; Spiess, H. W. *Macromolecules* **1992**, *25*, 3273.
(20) Wang, J. *J. Chem. Phys.* **1996**, *104*, 4850.
(21) Storey, R. F.; Chisholm, B. J.; Masse, M. A. *Polymer* **1996**, *37*, 2925.
(22) Zumbulyadis, N.; Landry, M. R.; Russel, T. P. *Macromolecules* **1996**, *29*, 2201.
(23) Wang, J.; Jack, K. S.; Natansohn, A. L. *J. Chem. Phys.* **1997**, *107*, 1016.
(24) Jack, K. S.; Wang, J.; Natansohn, A.; Register, R. A. *Macromolecules* **1998**, *31*, 3282.
(25) Klug, H. P.; Alexander, L. E. *X-ray Diffraction Procedures for Polycrystalline and Amorphous Materials*; John Wiley & Sons: New York, 1974.
(26) Feigin, L. A.; Svergun, D. I. *Structure Analysis by Small-Angle X-Ray and Neutron* Scattering; Plenum Press: New York, 1987.
(27) Hashimoto, T.; Fujimura, M.; Kawai, H. *Macromolecules* **1980**, *13*, 1660.

MA991974I